

# Explicit IMF $B_y$ -dependence of energetic protons and the ring current

L. Holappa<sup>1,2,3</sup>, N.Y. Buzulukova<sup>2,3</sup>

<sup>1</sup>Space Physics and Astronomy Research Unit, University of Oulu, Finland

<sup>2</sup>University of Maryland, College Park, MD, USA

<sup>3</sup>NASA Goddard Space Flight Center, Greenbelt, MD, USA

## Key Points:

- We show for the first time that there is an explicit  $B_y$ -dependence in the ring current/proton precipitation and in the inner magnetosphere.
- During NH summer (winter) the ring current fluxes/proton precipitation and the rate of change of the  $Dst$  index are stronger for  $B_y < 0$  ( $B_y > 0$ ).
- The  $B_y$ -dependence of the ring current and energetic proton fluxes is reproduced by a global coupled MHD-ring current model.

---

Corresponding author: Lauri Holappa, [lauri.holappa@oulu.fi](mailto:lauri.holappa@oulu.fi)

## Abstract

The most important parameter driving the solar wind-magnetosphere interaction is the southward ( $B_z$ ) component of the interplanetary magnetic field (IMF). While the dawn-dusk ( $B_y$ ) component of the IMF is also known to play an important role, its effects are usually assumed to be independent of its sign. Here we demonstrate for the first time a seasonally varying, explicit IMF  $B_y$ -dependence of the ring current and  $Dst$  index. Using satellite observations and a global magnetohydrodynamic (MHD) model coupled with a ring current model, we show that for a fixed level of solar wind driving the flux of energetic magnetospheric protons and the growth-rate of the ring current are greater for  $B_y < 0$  ( $B_y > 0$ ) than for  $B_y > 0$  ( $B_y < 0$ ) in Northern Hemisphere summer (winter). While the physical mechanism of this explicit  $B_y$ -effect is not yet fully understood, our results suggest that IMF  $B_y$  modulates magnetospheric convection and plasma transport in the inner magnetosphere.

## 1 Introduction

The interaction between solar wind, interplanetary magnetic field (IMF) and the Earth's magnetic field is dominated by the north-south ( $B_z$ ) component of IMF, which is the most important driver of dayside reconnection [Dungey, 1961], and thus the energy input into the magnetosphere. The dawn-dusk ( $B_y$ ) component of IMF is also known to play an important role, leading, e.g., to a  $B_y$ -dependence of the ionospheric convection patterns [Heppner and Maynard, 1987; Cowley et al., 1991; Ruohoniemi and Greenwald, 2005; Thomas and Shepherd, 2018]. It is also known that IMF  $B_y$  modulates the dayside reconnection rate by affecting, e.g., the geometry of the merging line [Sonnerup, 1974; Laitinen et al., 2007; Trattner et al., 2012], its effect on the magnetospheric response is usually assumed to be symmetric with respect to its sign. However, several studies [Friis-Christensen et al., 1972, 2017; Smith et al., 2017; Holappa and Mursula, 2018; Workayehu et al., 2021; Holappa et al., 2021] have shown that there is a strong IMF  $B_y$ -dependence in auroral currents which is not symmetric with the  $B_y$  sign. This so-called explicit  $B_y$ -dependence is especially strong in the  $AL$  index (measuring the westward electrojet), which is about 40% stronger for  $B_y > 0$  than for  $B_y < 0$  in Northern Hemisphere (NH) winter, or under negative tilt angle of the Earth's magnetic dipole with respect to the Sun-Earth line. In Northern Hemisphere summer (or during positive dipole tilt) the  $B_y$ -dependence is reversed.

The  $B_y$ -dependence of the auroral electrojets is at least partly due to a  $B_y$ -dependence of electron precipitation and ionospheric conductance. *Holappa et al.* [2020] showed that the fluxes of energetic ( $> 30$  keV) precipitating electrons in the dawn sector (measured by the National Oceanic and Atmospheric Administration (NOAA) Polar Operational Environmental satellites, POES) are modulated by IMF  $B_y$  similarly as the westward electrojet (greater precipitation for  $B_y < 0$  in NH summer and  $B_y > 0$  in NH winter). The  $B_y$ -dependence of electron precipitation implies a similar  $B_y$ -dependence of ionospheric conductance. Recent studies [*Holappa et al.*, 2021; *Weimer and Edwards*, 2021] have indeed found a similar IMF  $B_y$ -dependence of ionospheric conductance, maximizing in the dawn sector.

The physical mechanism of the explicit  $B_y$ -effect is still not fully understood. As the above recent studies indicate, understanding how IMF  $B_y$  modulates the magnetospheric energetic particles and their precipitation into ionosphere are of key importance. An important question is whether the ring current also exhibits an explicit  $B_y$ -dependence. Possible explicit IMF  $B_y$  effects in the inner magnetosphere have not been analyzed, although it has been suggested that IMF  $B_y$  plays a role in skewing of the inner magnetosphere electric field as observed in Energetic Neutral Atom (ENA) emissions [*C:son Brandt et al.*, 2002].

A viable method for studying the coupling between IMF  $B_y$  and the ring current is to use physics-based numerical models, such as global magnetohydrodynamic (MHD) models coupled with the ring current models of the inner magnetosphere [*de Zeeuw et al.*, 2004; *Tóth et al.*, 2005; *Zhang et al.*, 2007; *Buzulukova et al.*, 2010a; *Glocer et al.*, 2013]. While the MHD physics is not sufficient for describing energetic particle populations, the global MHD models can be coupled with kinetic inner magnetosphere models, such as the Comprehensive Inner Magnetosphere-Ionosphere (CIMI) model [*Fok et al.*, 2014, 2021], designed for modeling the ring current and radiation belt physics.

The goal of this paper is to quantify the  $B_y$ -dependence of magnetospheric electrons and protons and the ring current using global modeling with a coupled model and satellite measurements. We will use the Space Weather Modeling Framework (SWMF) [*Tóth et al.*, 2005] coupled with the CIMI model. With this capability we are able to model also the  $B_y$ -dependence of the ring current fluxes. We will compare the modeling results

to measurements of NOAA POES measurements of energetic magnetospheric protons and the *Dst* index.

This paper is organized as follows. In Section 2 we will introduce the data and the models in our analysis. The results from the global coupled model and satellite measurements are given in Sections 3 and 4, respectively. Finally we discuss our results and give our conclusions in Section 5.

## 2 Data and methods

### 2.1 Global 3D MHD BATS-R-US model coupled with CIMI

We use the global 3D BATS-R-US MHD code [Tóth *et al.*, 2005] coupled with the Comprehensive Inner Magnetosphere and Ionosphere (CIMI) model [Fok *et al.*, 2014] and Ridley ionospheric electrodynamics (RIM) module [Ridley *et al.*, 2004]. BATS-R-US and RIM are parts of Space Weather Modeling Framework (SWMF) developed at University of Michigan. The CIMI coupled code is developed at NASA GSFC Geospace Physics laboratory. For this study we use an ideal one-fluid anisotropic version of BATS-R-US MHD with grid resolution  $1/8 R_E$  in the near-Earth region. The total number of grid points is  $\sim 8 \times 10^6$ . It is acknowledged that magnetic field reconnection in ideal MHD model is defined by numerical resistivity, however multiple studies of substorms with different MHD codes [Fedder *et al.*, 1995; Raeder *et al.*, 2010; Birn and Hesse, 2013; Gordeev *et al.*, 2017; Merkin *et al.*, 2019; Keesee *et al.*, 2021] confirm that this approach works reasonably well for the Earth's magnetosphere (although with some caveats). Global MHD model provides a reasonable solution for 3D structure of currents, magnetic field and plasma parameters (bulk velocity, pressure and density). In the inner magnetosphere, additional physics should be included to describe the ring current effects. This is done by dynamic two-way coupling of MHD solution and the ring current solution in order to describe energy-dependent gradient drifts of the ring current population with energies  $\sim 1 - 200$  keV. Details of the coupling methodology can be found in [de Zeeuw *et al.*, 2004; Glozer *et al.*, 2013].

Solution for ionospheric electric field potential is provided by RIM with ionospheric conductivity calculated from an empirical relation between field-aligned currents and ionospheric conductivity specified with the Assimilative Mapping of Ionospheric Electrodynamics (AMIE) model [Ridley *et al.*, 2004].

In this paper we present the results of two runs with positive/negative IMF GSM  $B_y = +5/-5$  nT for the dipole tilt  $20^\circ$  in XZ GSM plane, corresponding to summer in northern hemisphere (NH). The value of tilt is kept fixed through the two runs. Except IMF  $B_y$  all run parameters are kept the same. Two runs are made with static IMF input solar wind  $V_x = -500$  km/sec;  $V_y = V_z = 0$ ; IMF  $B_x = 0$ ; solar wind density  $n=3$  cm<sup>3</sup>; solar wind temperature  $T = 200000$  K. The first 2h of simulations are done with  $B_z = 3$  nT, and the next 6h of simulations are done with static  $B_z = -5$  nT.

## 2.2 NOAA POES data and Dst index data

In this paper we use energetic particle measurements from NOAA15-NOAA19 satellites in 1995-2019. The measurements from different NOAA satellites have been calibrated for instrument degradation and other issues [Asikainen and Mursula, 2011, 2013]. The POES satellites measure protons with two orthogonal ( $0^\circ$  and  $90^\circ$ ) detectors, measuring both precipitating and trapped particles. To compare the POES measurements to the modeled omnidirectional proton fluxes we average the  $0^\circ$  and  $90^\circ$  fluxes of the lowest energy channel (30-80 keV).

To quantify the intensity of the ring current we use the *Dst* index. Instead of the standard (Kyoto) *Dst* index (which is currently only available until 2014 in the final form) we use the University of Oulu version (called the *Dxt* index, available at `dcx.oulu.fi`), which also corrects some minor errors in the standard *Dst* index [Karinen and Mursula, 2005; Mursula et al., 2008]. However, we note that practically identical results can be obtained using the standard *Dst* index.

## 3 Results: IMF $B_y$ effect in CIMI fluxes and energy content

Figure 1a and 1b show the omnidirectional fluxes of 56 keV protons for the last timestep (8.00 h) of the two runs at the geomagnetic equatorial plane (minimum B field plane) for  $B_y = +5$  nT and  $B_y = -5$  nT, respectively, calculated from CIMI output. For two runs with different  $B_y$  the proton flux is stronger in premidnight and dusk sectors. This reflects the well-known dawn-dusk asymmetry of the ring current during the storm main phase [Hamilton et al., 1988; Liemohn et al., 2001; Buzulukova et al., 2010b; Yakovchouk et al., 2012].

In addition to well-known dawn-dusk ring current asymmetry, proton fluxes in Figure 1 exhibit a strong  $B_y$ -dependence. The proton fluxes are greater for negative  $B_y$  than for positive  $B_y$ . This  $B_y$ -dependence is strongest in the dusk and premidnight sectors where the fluxes are also largest overall. Figure S1 in the supporting material is similar to Figure 1 shows that the omnidirectional (56 keV) electron flux in the dawn sector exhibits a similar  $B_y$ -dependence as protons in the dusk sector, showing larger value of fluxes for the run with negative  $B_y$ , in agreement with earlier based on NOAA POES measurements of  $> 30$  keV electrons [Holappa *et al.*, 2020].

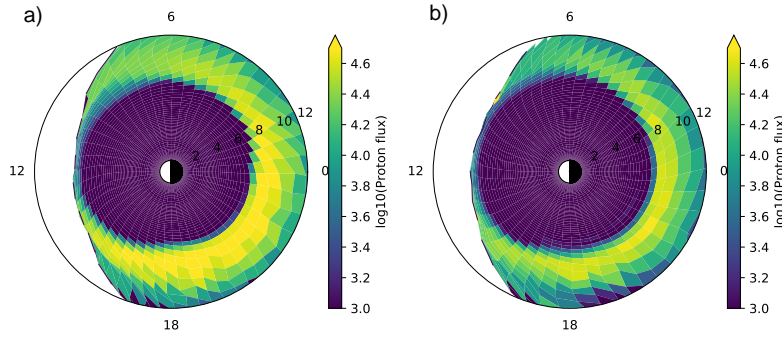


**Figure 1.** Equatorial omnidirectional fluxes of 56 keV protons for a) the run with  $B_y < 0$  b)  $B_y > 0$ . Flux units are  $1/cm^2/sr/s/keV$  in log-10 scale. The fluxes are shown for the last timesteps (8.00 h) of the two runs. Sun is from the left. Labels indicate magnetic local time and radial distance (in Earth radii).

Figure 2a shows the total energy content of the ring current calculated from the proton CIMI model for the two runs with opposite polarities of IMF  $B_y$  after the IMF  $B_z$  is turned southward at  $t = 2$  h. While the evolution of ring current energy is very similar for both signs of IMF  $B_y$  during  $t = 3.6$  h, negative  $B_y$  yields clearly greater ring current energy during the last two hours of the runs. The same  $B_y$ -dependence is seen in Figure 2b, which shows the pressure-corrected  $Dst$  indices ( $Dst^*$ ) [O'Brien and McPherron, 2000] calculated from the ring current energies ( $U$ ) in Figure 2a by the Dessler-Parker-Sckopke (DPS) relationship ( $Dst^* = 3.98 \cdot 10^{-30} \cdot U$  [keV]) [Dessler and Parker, 1959].

Both Figures 1 and 2 demonstrate that the ring current fluxes, energy content and the modeled  $Dst$  index show explicit IMF  $B_y$ -dependence with stronger ring current and larger fluxes for negative  $B_y$  in northern hemisphere summer.

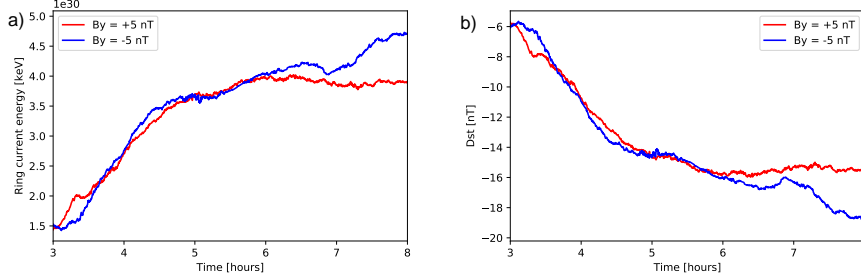


**Figure 2.** a) Simulated total energy of the ring current protons as a function of the simulation time for the signs of IMF  $B_y$ . b)  $Dst^*$  indices calculated from the total proton energy using the Dessler-Parker-Sckopke relationship.

#### 4 Results: IMF $B_y$ -effect in measured energetic protons and the $Dst$ index

To support and extend results presented in the previous section, we study the  $B_y$ -dependence of energetic (30-80 keV) protons, measured by NOAA POES satellites. For quantifying the  $B_y$ -dependence of the particle fluxes we use similar methodology as *Hollappa et al.* [2020], by sorting the measured particle fluxes by IMF  $B_y$  and the the *Newell et al.* [2007] coupling function, designed to represent the dayside reconnection rate at the magnetopause (MP)

$$\frac{d\Phi_{MP}}{dt} = v^{4/3} B_T^{2/3} \sin(\theta/2)^{8/3}, \quad (1)$$

where  $B_T = \sqrt{B_z^2 + B_y^2}$  and  $\theta = \arctan B_y/B_z$  is the IMF clock-angle. This coupling function is dominated by IMF  $B_z$ , but it also includes IMF  $B_y$ . However, the Newell function (as all other coupling functions) is symmetric with respect to the sign of  $B_y$ .

Figures 3a and 3b show the average 30-80 keV proton fluxes in both hemispheres under positive ( $> 20^\circ$ ) dipole tilt. The proton fluxes are averaged over the dusk sector (12-24 MLT) and  $\pm(55^\circ \dots 75^\circ)$  corrected geomagnetic latitude, roughly corresponding to  $L = 3-10$ , which are the MLT and  $L$ -ranges with highest fluxes of protons in the CIMI results in Figure 1. The proton fluxes are binned by the Newell coupling function  $d\Phi_{MP}/dt$  and IMF  $B_y$  averaged over 3 hours prior the proton measurements.

Figures 3a and 3b show that for a fixed value of  $d\Phi_{MP}/dt$ , the proton flux is clearly greater for  $B_y < 0$  than for  $B_y > 0$  in both hemispheres, in agreement with the above simulation results. The proton fluxes are generally higher in SH than NH, probably due to hemispheric asymmetry of magnetic field strength related to the South Atlantic Anomaly. Figures 3c and 3d further quantify the size of the  $B_y$ -dependence showing averages of the proton fluxes for  $B_y < 0$  and  $B_y > 0$  as a function of  $d\Phi_{MP}/dt$ . The standard errors in Figures 3c and 3d are calculated by normalizing the standard deviation on each bin by the square root of the number of samples. The  $B_y$ -effect is present in both hemispheres, although it is stronger for SH. Note that the flux units are shown in logarithmic scale.

Assuming that the fluxes measured by NOAA POES satellites (on low-Earth orbit) reflect patterns in underlying equatorial population, this result strongly supports the above CIMI results on  $B_y$  dependence of equatorial ring current fluxes.

Figure S2 in the supporting material shows the same analysis as Figure 3 for NH winter (dipole tilt  $< -20^\circ$ ). Figure S2 clearly shows that the  $B_y$ -dependence is reversed in the NH winter, in agreement with earlier studies on the explicit  $B_y$ -effect.

The above SWMF/CIMI model results also suggest that the  $Dst$  index exhibits an explicit  $B_y$ -dependence. To verify this, we make a similar analysis using the measured  $Dst$ ,  $Dst^*$  index and their rate of change. Figure 4a shows the average measured  $Dst$  index as a function of 3-hour means of  $d\Phi_{MP}/dt$  and IMF  $B_y$  during NH summer (dipole tilt  $> 20^\circ$ ) in the same format as in Figure 3. Figure 4a shows asymmetric pattern with respect to  $B_y$ , but the dependence is not so clear as for the proton precipitation. This is likely due to the long memory of the  $Dst$  index, that is, there is a large lag between solar wind driving (coupling functions) and the response of the  $Dst$  index, because the value of  $Dst$  index for any give hour is mainly determined by the pre-existing ring current population. However, the time-derivative of the  $Dst$  index is known to have a more immediate response [Burton *et al.*, 1975; Newell *et al.*, 2007]. Indeed, there is a clear  $B_y$ -dependence in  $\Delta Dst$  (Figure 4b), which is the change of the  $Dst$  index over three hours. The  $B_y$ -dependence of  $Dst$  and  $\Delta Dst$  are further quantified in Figures 4c and 4d, which show the averages of the  $Dst$  index and  $\Delta Dst$  for  $B_y < 0$  and  $B_y > 0$  during different values of  $d\Phi_{MP}/dt$ . Analysis of error bars indicates that the effect is stronger for  $\Delta Dst$  and more statistically significant, but it is still present for  $Dst$  index as well.

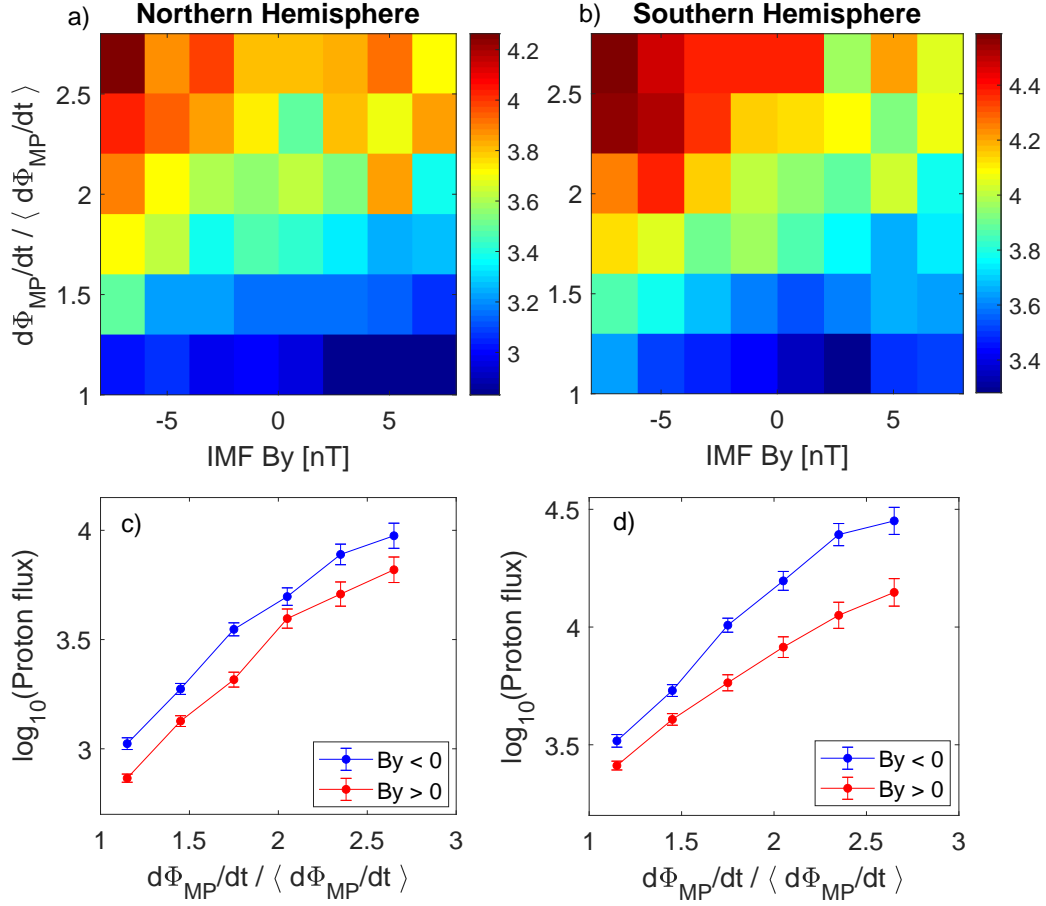


**Figure 3.** Flux of 30-80 keV protons measured by NOAA POES satellites as a function of 3-hour means of the Newell coupling function  $d\Phi_{MP}/dt$  and IMF  $B_y$  during NH summer conditions (dipole tilt  $> 20^\circ$ ) a) in Northern Hemisphere ( $55^\circ \dots 70^\circ$  corrected geomagnetic latitude) b) Southern Hemisphere ( $-55^\circ \dots -75^\circ$  corrected geomagnetic latitude). The units are  $1/\text{cm}^2/\text{sr}/\text{s}$  in log-10 scale. The Newell coupling function is normalized by its mean value in 1995-2019  $\langle d\Phi_{MP}/dt \rangle = 3.781 \cdot 10^3 \text{ (km/s)}^{4/3} \text{ nT}^2/3$ . c-d) Proton fluxes a-b) in averaged for  $B_y < 0$  and  $B_y > 0$  as a function of  $d\Phi_{MP}/dt$ . The vertical bars denote the standard errors of the means. Note the log scale for the proton flux.

Thus, the ring current grows at a faster rate ( $-\Delta Dst$  is greater) for  $B_y < 0$  during positive dipole tilt, confirming the CIMI modeling results on the ring current energy content and model  $Dst$  index (Fig. 2). Figures S3a and S3b show the same analysis of  $Dst$  and  $\Delta Dst$  for negative ( $< -20^\circ$ ) dipole tilt. The  $B_y$ -dependence during negative tilt is reversed (faster growth of the ring current for  $B_y > 0$ ) which is also expected from earlier studies on the explicit  $B_y$ -effects. The  $B_y$ -dependence in the time-derivative of

the  $Dst$ -index is quite strong. For the highest values of the Newell coupling function shown in Figure 4d  $\Delta Dst$  is about 50% greater for  $B_y < 0$  than for  $B_y > 0$ . In order to have sufficient statistics, data in Figure 4 are limited to mainly non-storm times (as seen in the scale of  $Dst$  values in Figure 4a). Further modeling and event studies are needed for studying how significant the  $B_y$ -dependence is during storm-times. Figures S3c-S3d and S3e-S3f repeat the analysis of Figure 4 for positive and negative dipole tilts using the pressure-corrected  $Dst$  index ( $Dst^*$ ) [O'Brien and McPherron, 2000], yielding practically identical results. This gives confidence that the results of Figure 4 are not contaminated by the magnetopause current.

Taken together, the analysis of NOAA POES data and  $Dst$  index gives strong evidence that there is a *global* explicit IMF  $B_y$ -effect in magnetospheric energetic protons and ring current energy content. These findings are strongly supported by the above SWMF/CIMI results as well.

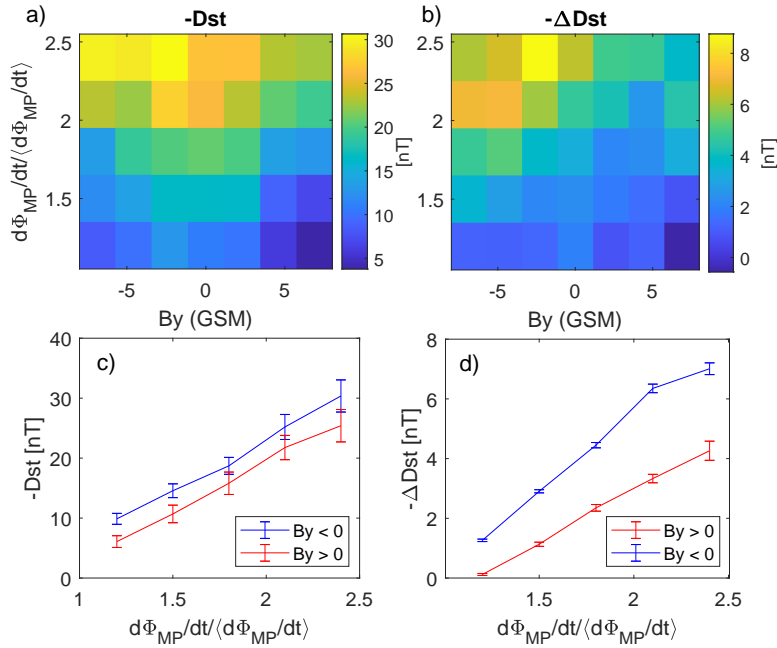


**Figure 4.** a) The  $Dst$  index as a function of 3-hour means of the Newell coupling function  $d\Phi_{MP}/dt$  and IMF  $B_y$  in NH summer (dipole tilt  $> 20^\circ$ ). b) The change of the  $Dst$  index ( $\Delta Dst$ ) during the same three-hour intervals as in the panel a). Bottom panels show c)  $Dst$  d)  $\Delta Dst$  averaged for  $B_y < 0$  (blue line) and  $B_y > 0$  (red line) as a function of  $\Phi_{MP}/dt$ . The vertical bars denote the standard errors of the means.

## 5 Discussion and Conclusions

It has been known for a long time that IMF  $B_y$  plays a role in solar wind-magnetosphere interaction which is seen, e.g., convection patterns in polar caps and auroral zones [Hepner and Maynard, 1987; Cowley *et al.*, 1991; Ruohoniemi and Greenwald, 1996, 2005; Thomas and Shepherd, 2018]. Recent studies have revealed that IMF  $B_y$  effects are complex and seasonally varying, showing dependence on the dipole tilt angle. The combined dependence on IMF  $B_y$  and the dipole tilt (also called the explicit  $B_y$ -dependence) strongly modulates auroral electrojets [Friis-Christensen *et al.*, 2017; Holappa and Mursula, 2018; Holappa *et al.*, 2021; Workayehu *et al.*, 2021], electron precipitation [Holappa *et al.*, 2020], and the size of polar cap [Reistad *et al.*, 2020]. These effects are quite significant, for example showing variations in the  $AL$  index up to 40% for opposite values of  $B_y$ .

In this paper, using a global MHD/ring current model and satellite measurements we have demonstrated, for the first time, a global explicit IMF  $B_y$ -dependence of the ring current proton fluxes, and the  $Dst$  index. We showed that IMF  $B_y$ -component significantly modulates energetic magnetospheric protons, the time-derivative of the  $Dst$  index and consequently the growth-rate of the ring current.

First we performed two simulations with the SWMF coupled with the CIMI inner magnetosphere model with static solar wind/IMF inputs ( $V = 500$  km/s,  $B_z = -5$  nT) and positive ( $+20^\circ$ ) dipole tilt. The two runs had identical solar wind inputs and other settings except for the sign of IMF  $B_y$ . We found that the run with negative  $B_y$  produced stronger fluxes of energetic protons in the inner magnetosphere.

To verify the model results we quantified the explicit  $B_y$ -dependence of the energetic (30–80 keV) magnetospheric proton fluxes measured by NOAA POES satellites flying on polar low-Earth orbits. We showed that for fixed value of the Newell solar wind coupling function ( $d\Phi_{MP}/dt$ ) the NOAA POES proton fluxes are greater for  $B_y < 0$  than for  $B_y > 0$  in northern hemisphere summer (dipole tilt  $> 20^\circ$ ). These empirical results are in excellent agreement with the model results, assuming that the proton fluxes measured by NOAA POES satellites on low-Earth orbit reflect the modeled equatorial ring current protons with similar energy (IMF  $B_y$  not significantly modulating the pitch-angle distribution).

Because the ring current is mainly carried by energetic protons in the inner magnetosphere, the above results indicate that the ring current energy content and the  $Dst$  index should also exhibit an explicit IMF  $B_y$  dependence. Indeed, we found that the SWMF/CIMI run with a negative IMF  $B_y$  produced a greater energy content of the ring current and a more negative modeled  $Dst$  index. To verify this empirically, we showed that for a fixed value of  $d\Phi_{MP}/dt$  the measured  $Dst$  index,  $Dst^*$  index and the time-derivative of  $Dst$  and  $Dst^*$  ( $\Delta Dst, \Delta Dst^*$ ) is more negative for  $B_y < 0$  during positive dipole tilt.

Thus, for fixed solar wind driving the ring current grows faster and becomes stronger for  $B_y < 0$  ( $B_y > 0$ ) in northern hemisphere summer (winter). Therefore the ring current growth-rate exhibits a similar explicit  $B_y$ -dependence as the westward electrojet [Hollappa and Mursula, 2018] and substorm occurrence frequency [Ohma et al., 2021].

The physical mechanism(s) of the explicit  $B_y$ -effects on the magnetospheric dynamics and particularly on the inner magnetosphere are still not fully understood. Recently, Reistad et al. [2020] showed that the polar cap area exhibits a similar explicit  $B_y$ -dependence: during positive tilt polar cap is larger for  $B_y < 0$  than for  $B_y > 0$  while the  $B_y$ -dependence is opposite for negative dipole tilt. They suggested that IMF  $B_y$  either modulates the dayside reconnection rate or the magnetotail response to solar wind driving. Evidence toward the former hypothesis was provided by Reistad et al. [2021] who showed that there is an explicit  $B_y$ -dependence in the cross-polar cap potential which is consistent with a similar  $B_y$ -dependence of the substorm occurrence frequency [Ohma et al., 2021].

The IMF  $B_y$ -dependence of the energetic proton fluxes and the ring current in the inner magnetosphere is probably closely related to the  $B_y$ -dependence of substorm activity, as substorms are known to cause injections of energetic particles into the inner magnetosphere [Mauk and McIlwain, 1974; Birn et al., 1998; Gkioulidou et al., 2014]. Another explanation is suggested by results from ring current models showing that electric field in the inner magnetosphere controls the strength of the ring current (e.g., Ebihara and Ejiri [2003]). In order to get stronger ring current in the coupled model, there should be stronger potential drop and stronger convection near the ring current model polar boundary, that is, on closed magnetic field lines. From this perspective it would be interesting to reanalyze the results of Cson Brandt et al. [2002] to examine if strong IMF  $B_y$  produces additional skewing of the electric field in the inner magnetosphere. Multiple studies confirm that the presence of IMF  $B_y$  is not needed for the skewing since it

is produced by the ring current itself [Wolf, 1983; Fok *et al.*, 2003; Ebihara and Fok, 2004; Buzulukova *et al.*, 2010b]. However, the results of our study suggest that indeed some additional effect is possible since the strength of the ring current is modulated by IMF  $B_y$ . At present, it is not clear why the convection on the closed field lines should be stronger when the signs of IMF  $B_y$  and dipole tilt are opposite. However the reproduction of the effect with the coupled SWMF/CIMI model demonstrates the potential of future modeling studies to uncover the physical mechanism of the explicit  $B_y$ -effect. Further modeling and event-based studies are also needed for studying how significant the explicit  $B_y$ -dependence of the ring current is during storm-times.

## Acknowledgments

We acknowledge the financial support by the Academy of Finland to the Postdoctoral Researcher project of LH (no. 322459). For N. B., this work has been partially supported by NASA grant 80NSSC19K0085. N.B. thanks ISSI in Bern Switzerland for support of the International Team N523 "Imaging the Invisible: Unveiling the Global Structure of Earth's Dynamic Magnetosphere". This work was carried out using the SWMF and BATS-R-US tools developed at the University of Michigan's Center for Space Environment Modeling (CSEM). The modeling tools are available through the University of Michigan for download under a user license. The open source version of SWMF could be downloaded from <https://github.com/MSTEM-QUDA>. CIMI model has been developed at NASA GSFC, Heliophysics division, Geospace Physics Laboratory. Computational resources supporting this work were provided by the NASA High-End Computing (HEC) Program through the NASA Advanced Supercomputing (NAS) Division at Ames Research Center.

## 6 Data availability statement

The solar wind data (solar wind speed and different components of IMF) were downloaded from the OMNI2 database (<http://omniweb.gsfc.nasa.gov/>). All the original POES/MEPED energetic particle data used here are archived in the NOAA/NGDC datasever (<http://www.ngdc.noaa.gov/stp/satellite/poes/index.html>). The University of Oulu  $Dst$  index was downloaded from <https://dcx.oulu.fi>. Model output used in production of Figures 1 and 2 have been made available online for download at Zenodo <https://zenodo.org/record/5893998.Yez5jVmxVEY>, DOI:10.5281/zenodo.5893998.

## References

- Asikainen, T., and K. Mursula (2011), Recalibration of the long-term NOAA/MEPED energetic proton measurements, *J. Atm. Sol.-Terr. Phys.*, *73*(2-3), 335–347.
- Asikainen, T., and K. Mursula (2013), Correcting the NOAA/MEPED energetic electron fluxes for detector efficiency and proton contamination, *J. Geophys. Res.*, *118*(10), 6500–6510.
- Birn, J., and M. Hesse (2013), The substorm current wedge in mhd simulations, *Journal of Geophysical Research: Space Physics*, *118*(6), 3364–3376, doi: <https://doi.org/10.1002/jgra.50187>.
- Birn, J., M. F. Thomsen, J. E. Borovsky, G. D. Reeves, D. J. McComas, R. D. Belian, and M. Hesse (1998), Substorm electron injections: Geosynchronous observations and test particle simulations, , *103*(A5), 9235–9248, doi:10.1029/97JA02635.
- Burton, R. K., R. L. McPherron, and C. T. Russell (1975), An empirical relationship between interplanetary conditions and dst, *J. Geophys. Res.*, *80*(31), 4204–4214.
- Buzulukova, N., M.-C. Fok, A. Pulkkinen, M. Kuznetsova, T. E. Moore, A. Gloer, P. C. Brandt, G. Toth, and L. Rastätter (2010a), Dynamics of ring current and electric fields in the inner magnetosphere during disturbed periods: CRCM–BATS-R-US coupled model, *J. Geophys. Res. Space Physics*, *115*(A5).
- Buzulukova, N., M.-C. Fok, J. Goldstein, P. Valek, D. J. McComas, and P. C. Brandt (2010b), Ring current dynamics in moderate and strong storms: Comparative analysis of twins and image/hena data with the comprehensive ring current model, *Journal of Geophysical Research: Space Physics*, *115*(A12), doi: <https://doi.org/10.1029/2010JA015292>.
- Cowley, S. W. H., J. P. Morelli, and M. Lockwood (1991), Dependence of convective flows and particle precipitation in the high-latitude dayside ionosphere on the x and y components of the interplanetary magnetic field, *J. Geophys. Res.*, *96*(A4), 5557–5564.
- C:son Brandt, P., S. Ohtani, D. G. Mitchell, M.-C. Fok, E. C. Roelof, and R. Demajistre (2002), Global ena observations of the storm mainphase ring current: Implications for skewed electric fields in the inner magnetosphere, *Geophysical Research Letters*, *29*(20), 15–1–15–3, doi:<https://doi.org/10.1029/2002GL015160>.

- de Zeeuw, D. L., S. Sazykin, R. A. Wolf, T. I. Gombosi, A. J. Ridley, and G. Tóth (2004), Coupling of a global MHD code and an inner magnetospheric model: Initial results, *Journal of Geophysical Research (Space Physics)*, *109*(A12), A12219, doi:10.1029/2003JA010366.
- Dessler, A. J., and E. N. Parker (1959), Hydromagnetic theory of geomagnetic storms, *J. Geophys. Res.*, *64*(12), 2239–2252.
- Dungey, J. W. (1961), Interplanetary magnetic field and the auroral zones, *Phys. Rev. Lett.*, *6*, 47–49.
- Ebihara, Y., and M. Ejiri (2003), Numerical Simulation of the Ring Current: Review, *J. Geophys. Res.*, *108*(1), 377–452, doi:10.1023/A:1023905607888.
- Ebihara, Y., and M. C. Fok (2004), Postmidnight storm-time enhancement of tens-of-keV proton flux, *Journal of Geophysical Research (Space Physics)*, *109*(A12), A12209, doi:10.1029/2004JA010523.
- Fedder, J. A., S. P. Slinker, J. G. Lyon, and R. D. Elphinstone (1995), Global numerical simulation of the growth phase and the expansion onset for a substorm observed by viking, *Journal of Geophysical Research: Space Physics*, *100*(A10), 19,083–19,093, doi:https://doi.org/10.1029/95JA01524.
- Fok, M. C., T. E. Moore, G. R. Wilson, J. D. Perez, X. X. Zhang, P. C. S. Brandt, D. G. Mitchell, E. C. Roelof, J. M. Jahn, C. J. Pollock, and R. A. Wolf (2003), Global ena Image Simulations, *J. Geophys. Res.*, *108*(1), 77–103, doi:10.1023/B:SPAC.0000007514.56380.f0.
- Fok, M.-C., N. Y. Buzulukova, S.-H. Chen, A. Gloer, T. Nagai, P. Valek, and J. D. Perez (2014), The comprehensive inner magnetosphere-ionosphere model, *J. Geophys. Res. Space Physics*, *119*(9), 7522–7540.
- Fok, M.-C., S.-B. Kang, C. P. Ferradas, N. Y. Buzulukova, A. Gloer, and C. M. Komar (2021), New Developments in the Comprehensive Inner Magnetosphere-Ionosphere Model, *J. Geophys. Res. Space Physics*, *126*(4), e2020JA028,987.
- Friis-Christensen, E., K. Lassen, J. Wilhjelm, J. M. Wilcox, W. Gonzalez, and D. S. Colburn (1972), Critical component of the interplanetary magnetic field responsible for large geomagnetic effects in the polar cap, *J. Geophys. Res.*, *77*(19), 3371–3376, doi:10.1029/JA077i019p03371.
- Friis-Christensen, E., C. C. Finlay, M. Hesse, and K. M. Laundal (2017), Magnetic Field Perturbations from Currents in the Dark Polar Regions During Quiet Geo-

- 403 magnetic Conditions, *Space Sci. Rev.*, *206*(1-4), 281–297.
- 404 Gkioulidou, M., A. Y. Ukhorskiy, D. G. Mitchell, T. Sotirelis, B. H. Mauk, and L. J.
- 405 Lanzerotti (2014), The role of small-scale ion injections in the buildup of Earth’s
- 406 ring current pressure: Van Allen Probes observations of the 17 March 2013 storm,
- 407 *J. Geophys. Res. Space Physics*, *119*(9), 7327–7342.
- 408 Glocer, A., M. Fok, X. Meng, G. Toth, N. Buzulukova, S. Chen, and K. Lin (2013),
- 409 CRCM+ BATS–R–US two–way coupling, *J. Geophys. Res. Space Physics*, *118*(4),
- 410 1635–1650.
- 411 Gordeev, E., V. Sergeev, N. Tsyganenko, M. Kuznetsova, L. Rastätter, J. Raeder,
- 412 G. Tóth, J. Lyon, V. Merkin, and M. Wiltberger (2017), The substorm cy-
- 413 cle as reproduced by global mhd models, *Space Weather*, *15*(1), 131–149, doi:
- 414 <https://doi.org/10.1002/2016SW001495>.
- 415 Hamilton, D. C., G. Gloeckler, F. Ipavich, W. Stüdemann, B. Wilken, and
- 416 G. Kremser (1988), Ring current development during the great geomagnetic storm
- 417 of february 1986, *J. Geophys. Res.*, *93*(A12), 14,343–14,355.
- 418 Heppner, J. P., and N. C. Maynard (1987), Empirical high-latitude electric field
- 419 models, *J. Geophys. Res.*, *92*(A5), 4467–4489.
- 420 Holappa, L., and K. Mursula (2018), Explicit IMF  $B_y$ -dependence in high-
- 421 latitude geomagnetic activity, *J. Geophys. Res.*, *123*, 4728–4740, doi:
- 422 [10.1029/2018JA025517](https://doi.org/10.1029/2018JA025517).
- 423 Holappa, L., T. Asikainen, and K. Mursula (2020), Explicit IMF Dependence in Ge-
- 424 omagnetic Activity: Modulation of Precipitating Electrons, *Geophys. Res. Lett.*,
- 425 *47*(4), e2019GL086,676.
- 426 Holappa, L., R. M. Robinson, A. Pulkkinen, T. Asikainen, and K. Mursula (2021),
- 427 Explicit IMF  $B_y$ -Dependence in Geomagnetic Activity: Quantifying Ionospheric
- 428 Electrodynamics, *J. Geophys. Res. Space Physics*, *126*(4), e2021JA029,202.
- 429 Karinen, A., and K. Mursula (2005), A new reconstruction of the Dst index for
- 430 1932-2002, *Ann. Geophys.*, *23*, 475–485.
- 431 Keesee, A. M., N. Buzulukova, C. Mouikis, and E. E. Scime (2021), Mesoscale
- 432 structures in earth’s magnetotail observed using energetic neutral atom
- 433 imaging, *Geophysical Research Letters*, *48*(3), e2020GL091,467, doi:
- 434 <https://doi.org/10.1029/2020GL091467>, e2020GL091467 2020GL091467.

- 435 Laitinen, T. V., M. Palmroth, T. I. Pulkkinen, P. Janhunen, and H. E. J. Koskinen  
 436 (2007), Continuous reconnection line and pressure-dependent energy conversion on  
 437 the magnetopause in a global mhd model, *J. Geophys. Res.*, *112*(A11).
- 438 Liemohn, M. W., J. U. Kozyra, M. F. Thomsen, J. L. Roeder, G. Lu, J. E.  
 439 Borovsky, and T. E. Cayton (2001), Dominant role of the asymmetric ring cur-  
 440 rent in producing the stormtime dst, *J. Geophys. Res. Space Physics*, *106*(A6),  
 441 10,883–10,904.
- 442 Mauk, B. H., and C. E. McIlwain (1974), Correlation of Kp with the substorm-  
 443 injected plasma boundary, , *79*(22), 3193–3196, doi:10.1029/JA079i022p03193.
- 444 Merkin, V. G., E. V. Panov, K. A. Sorathia, and A. Y. Ukhorskiy (2019), Contri-  
 445 bution of bursty bulk flows to the global dipolarization of the magnetotail during  
 446 an isolated substorm, *Journal of Geophysical Research: Space Physics*, *124*(11),  
 447 8647–8668, doi:https://doi.org/10.1029/2019JA026872.
- 448 Mursula, K., L. Holappa, and A. Karinen (2008), Correct normalization of the Dst  
 449 index, *Astrophys. Space Sci. Transact.*, *4*, 41–45, doi:10.5194/astra-4-41-2008.
- 450 Newell, P. T., T. Sotirelis, K. Liou, C.-I. Meng, and F. J. Rich (2007), A nearly  
 451 universal solar wind-magnetosphere coupling function inferred from 10 magneto-  
 452 spheric state variables, *J. Geophys. Res.*, *112*(A1).
- 453 O’Brien, T. P., and R. L. McPherron (2000), An empirical phase space analysis of  
 454 ring current dynamics: Solar wind control of injection and decay, *J. Geophys. Res.*  
 455 *Space Physics*, *105*(A4), 7707–7719.
- 456 Ohma, A., J. P. Reistad, and S. M. Hatch (2021), Modulation of Magnetospheric  
 457 Substorm Frequency: Dipole Tilt and IMF By Effects, *J. Geophys. Res. Space*  
 458 *Physics*, *126*(3), e2020JA028,856.
- 459 Raeder, J., P. Zhu, Y. Ge, and G. Siscoe (2010), Open geospace general circulation  
 460 model simulation of a substorm: Axial tail instability and ballooning mode pre-  
 461 ceding substorm onset, *Journal of Geophysical Research: Space Physics*, *115*(A5),  
 462 doi:https://doi.org/10.1029/2010JA015876.
- 463 Reistad, J. P., K. M. Laundal, A. Ohma, T. Moretto, and S. E. Milan (2020), An  
 464 Explicit IMF By Dependence on Solar Wind-Magnetosphere Coupling, *Geophys.*  
 465 *Res. Lett.*, *47*(1), e2019GL086,062.
- 466 Reistad, J. P., K. M. Laundal, N. Østgaard, A. Ohma, A. G. Burrell, S. M. Hatch,  
 467 S. Haaland, and E. G. Thomas (2021), Quantifying the lobe reconnection rate

- during dominant IMF by periods and different dipole tilt orientations, *J. Geophys. Res. Space Physics*, p. e2021JA029742.
- Ridley, A. J., T. I. Gombosi, and D. L. DeZeeuw (2004), Ionospheric control of the magnetosphere: conductance, *Annales Geophysicae*, *22*(2), 567–584, doi:10.5194/angeo-22-567-2004.
- Ruohoniemi, J. M., and R. A. Greenwald (1996), Statistical patterns of high-latitude convection obtained from Goose Bay HF radar observations, *J. Geophys. Res.*, *101*(A10), 21,743–21,763, doi:10.1029/96JA01584.
- Ruohoniemi, J. M., and R. A. Greenwald (2005), Dependencies of high-latitude plasma convection: Consideration of interplanetary magnetic field, seasonal, and universal time factors in statistical patterns, *J. Geophys. Res.*, *110*(A9).
- Smith, A. R. A., C. D. Beggan, S. Macmillan, and K. A. Whaler (2017), Climatology of the auroral electrojets derived from the along-track gradient of magnetic field intensity measured by POGO, Magsat, CHAMP, and Swarm, *Space Weather*, *15*(10), 1257–1269, doi:10.1002/2017SW001675, 2017SW001675.
- Sonnerup, B. U. O. (1974), Magnetopause reconnection rate, *J. Geophys. Res.*, *79*(10), 1546–1549, doi:10.1029/JA079i010p01546.
- Thomas, E. G., and S. G. Shepherd (2018), Statistical patterns of ionospheric convection derived from mid-latitude, high-latitude, and polar SuperDARN HF radar observations, *J. Geophys. Res.*, *123*(4), 3196–3216.
- Tóth, G., I. V. Sokolov, T. I. Gombosi, D. R. Chesney, C. R. Clauer, D. L. De Zeeuw, K. C. Hansen, K. J. Kane, W. B. Manchester, R. C. Oehmke, et al. (2005), Space Weather Modeling Framework: A new tool for the space science community, *J. Geophys. Res.*, *110*(A12).
- Trattner, K. J., S. M. Petrinec, S. A. Fuselier, and T. D. Phan (2012), The location of reconnection at the magnetopause: Testing the maximum magnetic shear model with THEMIS observations, *J. Geophys. Res. Space Physics*, *117*(A1).
- Weimer, D., and T. Edwards (2021), Testing the electrodynamic method to derive height-integrated ionospheric conductances, *Ann. Geophys.*, *39*(1), 31–51.
- Wolf, R. A. (1983), The quasi-static (slow-flow) region of the magnetosphere, in *Solar-Terrestrial Physics: Principles and Theoretical Foundations, Astrophysics and Space Science Library*, vol. 104, edited by R. L. Carovillano and J. M. Forbes, pp. 303–368, doi:10.1007/978-94-009-7194-3\_14.

- 501 Workayehu, A. B., H. Vanhamäki, A. T. Aikio, and S. G. Shepherd (2021), Effect of  
502 Interplanetary Magnetic Field on Hemispheric Asymmetry in Ionospheric Horizon-  
503 tal and Field-Aligned Currents During Different Seasons, *J. Geophys. Res. Space*  
504 *Physics*, *126*(10), e2021JA029,475.
- 505 Yakovchouk, O. S., K. Mursula, L. Holappa, I. S. Veselovsky, and A. Karinen (2012),  
506 Average properties of geomagnetic storms in 1932-2009, *J. Geophys. Res.*, *117*,  
507 A03201, doi:10.1029/2011JA017093.
- 508 Zhang, M. W., J. and Liemohn, D. L. De Zeeuw, J. E. Borovsky, A. J. Ridley,  
509 G. Toth, S. Sazykin, M. F. Thomsen, J. U. Kozyra, and T. I. Gombosi (2007),  
510 Understanding storm-time ring current development through data-model compar-  
511 isons of a moderate storm, *J. Geophys. Res. Space Physics*, *112*(A4).